Noncovalent Integration of a Bioinspired Ni Catalyst to Graphene Acid for Reversible Electrocatalytic Hydrogen Oxidation.

Bertrand Reuillard, Matías Blanco, Laura Calvillo, Nathan Coutard, Ahmed Ghedjatti, Pascale Chenevier, Stefano Agnoli, Michal Otyepka, Gaetano Granozzi, Vincent Artero

▶ To cite this version:

HAL Id: hal-02468287
https://hal.archives-ouvertes.fr/hal-02468287

Submitted on 5 Feb 2020

Non-covalent integration of a bio-inspired Ni catalyst to graphene acid for reversible electrocatalytic hydrogen oxidation

Bertrand Reuillard,[a] Matías Blanco,[b] Laura Calvillo,[b] Nathan Coutard,[a] Ahmed Ghedjatti,[a] Pascale Chenevier,[c] Stefano Agnoli,[b] Michal Otyepka,[d] Gaetano Granozzi[c] and Vincent Artero[a*]

a. Univ. Grenoble Alpes, CEA, CNRS, IRIG, Laboratoire de Chimie et Biologie des Métaux, F-38000 Grenoble.

b. Department of Chemical Sciences, University of Padova, Via Marzolo 1, 35131 Padova.

c. Univ. Grenoble Alpes, CEA, CNRS, IRIG, SYMMES, F-38000 Grenoble.

d. Regional Centre of Advanced Technologies and Materials, Department of Physical Chemistry, Palacký University Olomouc, 17. listopadu 1192/12, 771 46 Olomouc, Czech Republic

Abstract

Efficient heterogeneous catalysis of hydrogen oxidation reaction (HOR) by platinum group metal (PGM)-free catalysts in proton-exchange membrane (PEM) fuel cells represents a significant challenge towards the development of a sustainable hydrogen economy. Here we show that

graphene acid can be used as electrode scaffold for the non-covalent immobilization of a bio-inspired nickel bis-diphosphine HOR catalyst. The highly functionalized structure of this material and optimization of the electrode-catalyst assembly sets new benchmark electrocatalytic performances for heterogeneous molecular HOR, with current densities above 30 mA cm^{-2} at 0.4V vs RHE in acidic aqueous conditions and at room temperature. This study also shows the great potential of graphene acid for catalyst loading improvement and porosity management within nanostructured electrodes towards achieving high current densities with noble-metal free molecular catalyst.

Introduction

The use of hydrogen as a sustainable energy vector requires the development of efficient, low-cost but robust means to produce and oxidize H_2 at the cathode of electrolyzers and anode of fuel cells, respectively.[1,2] In state-of-the-art proton exchange membrane fuel cells (PEM-FC), the hydrogen oxidation reaction (HOR) is performed using scarce and expensive Pt- or Pt group metals (PGM) catalysts, which are critical raw materials, thus severely hampering their future deployment.[3–6] In recent years, several studies have reported the use of PGM-free catalyst for HOR, in particular with Ni-based materials under alkaline conditions[7–9] and metal-carbide based materials in acidic media.[10–14] Although some of these non-PGM based materials could demonstrate good activities for HOR with good resistance to poisoning, they still suffer from limited stability under operation.

Nature's catalysts for reversible H_2 production and oxidation, hydrogenases (H_2ase), are able to perform these reactions with very high TOFs (up to 10000 s^{-1}) using only cheap and widely available Fe and Ni metals at their catalytic site.[15–17] Despite their sensitivity to a number of

inhibitors and their high molecular weight, these enzymes have been extensively used for their impressive electrocatalytic properties in H_2-O_2 biofuel cells over the past decade.[18–20] Strategies involving the use of protecting redox polymer,[21–23] protein-surface orientation[24–26] or electrode nanostructuration[27,28] have been developed to overcome H_2ases intrinsic limitations. However, their fragility and sensitivity to various conditions and inhibitors combined with their large molecular footprint remain problematic for catalyst loading optimization and implementation in market-ready PEMFC setup.

Nevertheless, H_2ases have provided synthetic chemists with valuable blueprints that allowed synthesizing biomimetic and bio-inspired PGM-free compounds able to electrocatalytically generate and/or oxidize H_2.[29–33] In particular, the family of mononuclear Ni-based bis-diphosphine $[Ni(P_2^R N_2^{R'})_2]^{2+}$ complex first described by the DuBois's group represents a unique class of bidirectional molecular catalysts for electrocatalytic H_2/H^+ interconversion.[34–36] The 1,5- diaza- 3,7- diphosphacyclooctane ligand $(P_2^R N_2^{R'})$ provides an electron rich environment to the metal center while mimicking the 2- azapropanedithiolate bridge found in [FeFe]-H_2ases and acting as proton shuttle.[37–40] Over the past decade, an extensive body of work has focused on the expansion of the outer coordination sphere beyond the cyclic tertiary amine, in particular through the incorporation of amino acid residues to the ligand.[41–44] This allowed the design of an arginine containing derivative $[Ni^{II}(P_2^{Cy} N_2^{Arg})_2]^{7+}$ (**NiArg**) owing the strongest bias for HOR of the series, with reported TOFs up to 106 s^{-1} under 100 bar of H_2 at 72°C, while also retaining catalytic reversibility for H_2/H^+ interconversion over a broad pH range (Figure 1a).[45–47]

In order to reach technological relevance, molecular catalysts for fuel cells or solar fuels production need to be integrated onto electrode surfaces before being eventually implemented into functional devices.[48] This relatively recent research field has been particularly active over

the past few years.[49–51] Past developments of covalent or non-covalent grafting strategies for molecular catalyst have allowed great control over catalyst concentration at the material-electrolyte interface,[52,53] electrode-catalyst electron transfer rates and redox properties,[54–56] catalyst activity and stability[57–61] as well as in some cases catalyst selectivity,[62–64] through the possibility to tune its direct environment.

In particular, over the last decade efforts have focused on interfacing this series of Ni-based molecular catalysts with carbon-based electrodes for the development of molecular HER cathodes and HOR anodes.[65–70] Covalent or non-covalent modifications of carbon nanotube (CNT) electrodes with $[Ni(P_2^RN_2^{R'})_2]^{2+}$ allowed to reach current densities of 1-2 mA cm^{-2} measured at 0.3 V vs RHE and room temperature in 0.5 M H_2SO_4 for HOR.[65,66] Recent works reported improved performances reaching current densities up to 16 mA cm^{-2}, at 0.3 V vs RHE, through design and structuration of the CNT based electrodes.[68,69] Importantly, such bio-inspired electrodes are tolerant to CO,[66] compatible with proton-exchange membrane (PEM) technology[6] and they have been successfully integrated into fully functional proof-of-concept fuel cell devices.[69,71,72]
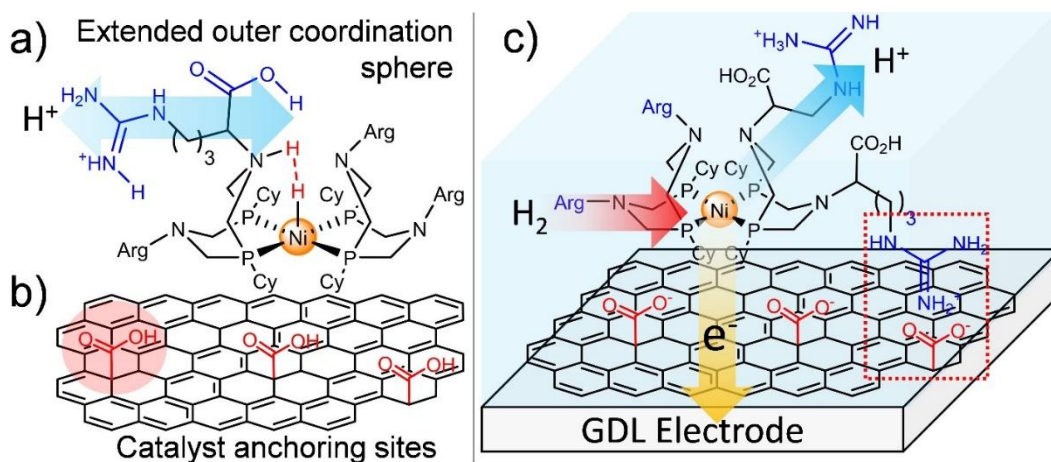
Figure 1: schematic representations of a) **NiArg** simplified chemical structure b) GA sheets bearing –CO$_2$H anchoring functions and c) the GA|**NiArg** composite modified electrode

In this context, graphene acid (GA) has recently appeared as a particularly appealing platform material for catalysis as it can be easily obtained from commercially available fluorographite. It yields material with high levels of carboxyl functionalization, about 10% (atomic content), directly grafted on the basal plane, allowing the graphene sheet to maintain excellent electron conduction properties (Figure 1b).[73] These properties were very recently exploited in order to covalently incorporate redox centers through peptide coupling or bind metal nanoparticles in order to perform C-H bond insertion, C-C bond coupling or even alcohol oxidation through heterogeneous catalytic processes.[74–76]

In here, we describe the use of GA nanosheets as an original electrode material for the non-covalent grafting of **NiArg** through electrostatic interactions. The highly functionalized and conductive GA provided a large amount of anchoring sites for the catalyst while ensuring excellent electronic wiring of the molecular catalyst, thus allowing the development of an efficient molecular-based anode for HOR in PEM fuel cells (Figure 1c).

Results and discussion

GA synthesis was carried out as previously reported[73] and the GA modified electrodes were prepared through vacuum filtration of a 0.05 mg mL^{-1} of GA dispersion in EtOH directly at the surface of a gas diffusion layer (GDL) coated with an hydrophobic microporous layer (MPL) (area = 10 cm^2). The volume of GA dispersion filtrated was varied in order to obtain several GA loadings (from 0.05 to 0.8 mg cm^{-2} of GA, see experimental part). The obtained GDL|GA films were characterized before and after modification with **NiArg** using X-ray photoelectron

spectroscopy and scanning electron microscopy (SEM) coupled with energy dispersive X-ray spectroscopy (EDX) mapping (Figure 2).
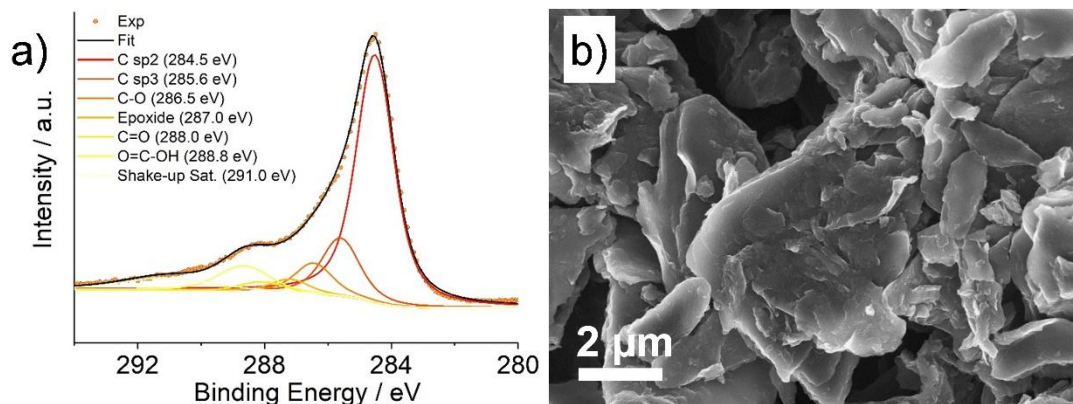

Figure 2: a) C 1s XPS region of GA sample b) SEM micrograph of a GA film deposited at the surface of a GDL

The C 1s XPS region spectra of the GA sample shows an important contribution of the carboxylic groups (Figure 2a). This high content in $-CO_2H$ functions (9.9 % atomic content determined by XPS, see Table S1) is expected to lead to an efficient grafting of **NiArg** at the electrode surface through electrostatic interactions with the guanidinium moieties of the catalyst. SEM characterization depicted flake-type microstructures for the GA deposit, with sheets size reaching up to several μm (Figure 2b and S1). EDX mapping of the films clearly shows high oxygen content on the GA surface where much lower levels are observed on the MPL layer part (Figure S2).

Catalyst deposition was carried out by drop casting 2 μL of a 5 mM concentration of **NiArg** in deionized water at the surface of the GDL|GA electrode surfaces of different thicknesses (area = 0.125 cm^2) (see SI for experimental details). The deposit was then dried for 10 min, before being rinsed with deionized water to remove unbound catalyst. The modified electrodes were

characterized using cyclic voltammetry (CV) in 0.5M H_2SO_4 with a constant flow of H_2 (5 mL min^{-1}) at the back of the GDL-based homemade working breathing electrode (Figure S3). For all modified electrodes, similar S-shape CV traces could be observed, characteristic of the catalytic behavior of **NiArg** for reversible H_2 production and oxidation in aqueous conditions, with a strong bias for HOR, as previously reported (Figure 3a).[69] During turnover and following the addition of H_2, the catalyst is thought to be reduced from Ni^{II} to Ni^{II}-H (with a protonated pendant amine) before being re-oxidized in a two-electrons process at the electrode, giving rise to the observed catalytic current.[45,46,69]
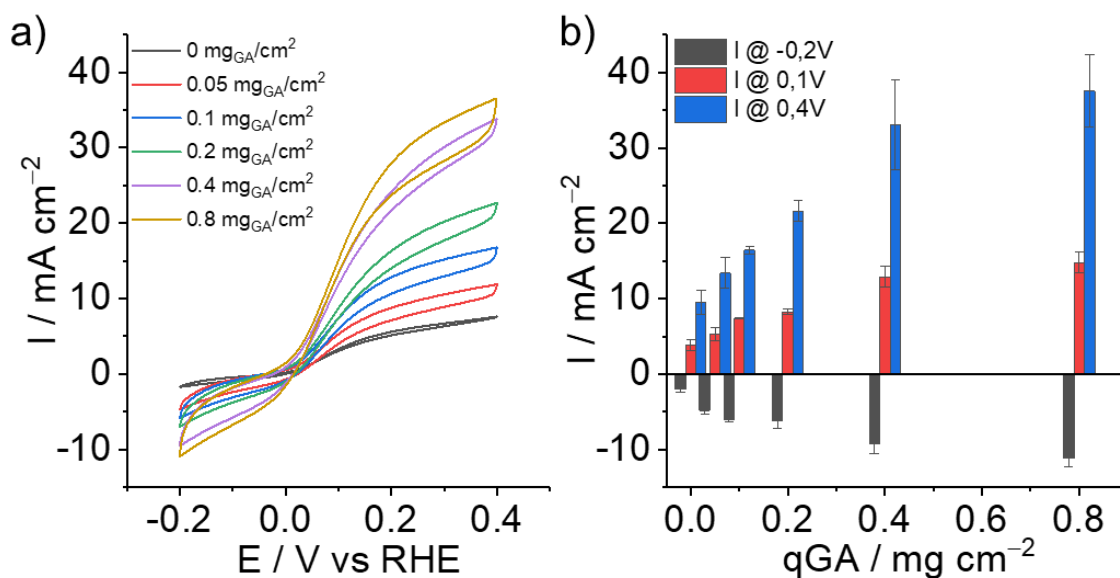

Figure 3: a) CV traces of GDL|GA electrodes at different GA loadings (0; 0.05; 0.1; 0.2; 0.4 and 0.8 mg cm^{-2}) modified with 2 µL of **NiArg** (5 mM) and b) current densities for HER at -0.2 V vs RHE and HOR at 0.1 and 0.4 V vs RHE obtained from CVs in 0.5 M H_2SO_4 with a constant flow of H_2 at the back of the GDL (5 mL min^{-1}) ($v = 20$ mV s^{-1})

As expected, direct deposition of catalyst on an unmodified GDL electrode leads to the lowest electrocatalytic responses (9 ± 2 mA cm^{-2} at 0.4V vs RHE). For the GDL|GA|**NiArg** electrodes, catalytic current responses scaled up almost linearly with the GA loading GDL before levelling

off at 0.4 mg cm^{-2} of GA giving maximum current densities for HOR of 33 ± 6 mA cm^{-2} at 0.4 V vs RHE setting up a new benchmark for molecular HOR. (Figure 3b). Maximum HOR current densities of 37 ± 5 mA cm^{-2} were obtained at 0.4 V vs RHE with 0.8 mg cm^{-2} of GA films but they showed limited mechanical stability during catalyst deposition and electrochemical testing due to material leaching off the electrode surface. Bare GA electrode, as well as GA electrode modified with Ni nanoparticles did not show any HOR activity (Figure S4a). Although still not competing with low-loaded Pt electrodes (Figure S4b), GDL|GA|**NiArg** electrodes outperform all previously reported bioinspired nanomaterials for catalytic HOR under acidic conditions.

In order to study the impact of the amount of catalyst deposited at the GDL|GA (0.4 mg cm^{-2}) electrode surface on HOR catalysis, concentration of **NiArg** in the deposition solution was varied from 1.25 to 10 mM. CVs performed in neutral buffer conditions (0.2M potassium phosphate, pH7) and under argon allowed to observe the reversible redox signature of **NiArg** at $E_{1/2} = 0.03$ V vs RHE corresponding to the 2e$^-$/2H$^+$ Ni-centered redox process (Fig 4a) as previously reported.[69] Integration of the oxidation wave allowed to estimate the catalyst loading ($\Gamma_{\mathbf{NiArg}}$) ranging from 9 nmol cm^{-2} to about 19 nmol cm^{-2}, depending on the concentration of **NiArg** deposited for the GLD|GA with 0.4 mg cm^{-2} of GA deposited (Figure 4b). Higher amounts of Ni (from 14 ± 3 to 45 ± 3 nmol cm^{-2}) were quantified from digested GDL|GA|**NiArg** films in nitric acid using inductively coupled plasma atomic emission spectroscopy (ICP-AES). These results indicate that only a part (~40%) of the overall grafted catalyst (detected by ICP) is electrochemically active (detected by CV). XPS measurements (Table S2) on the modified film confirmed the presence of Ni at the surface of the electrode and EDX mapping could show that **NiArg** was mainly grafted on the GA modified surface, as expected from the high surface concentration of –CO$_2$H groups (Figure S2b). As a result of the drop cast and drying method

used to deposit the catalyst, some non-specific interactions can potentially be expected. Thus this would explain the presence of small amounts of Ni on the hydrophobic MPL as well as formation of aggregates as seen on Figure S2c (although uneven distribution shown by EDX could potentially be caused by degradation under the electron beam). Interestingly, the amount of Ni measured by ICP-AES after 10 cycles of CVs under electrocatalytic conditions (Figure 4b) is closer to the one measured by CV and thus indicates a slow leaching of the catalyst out of the GA film in the electrolyte over the course of time and operation.
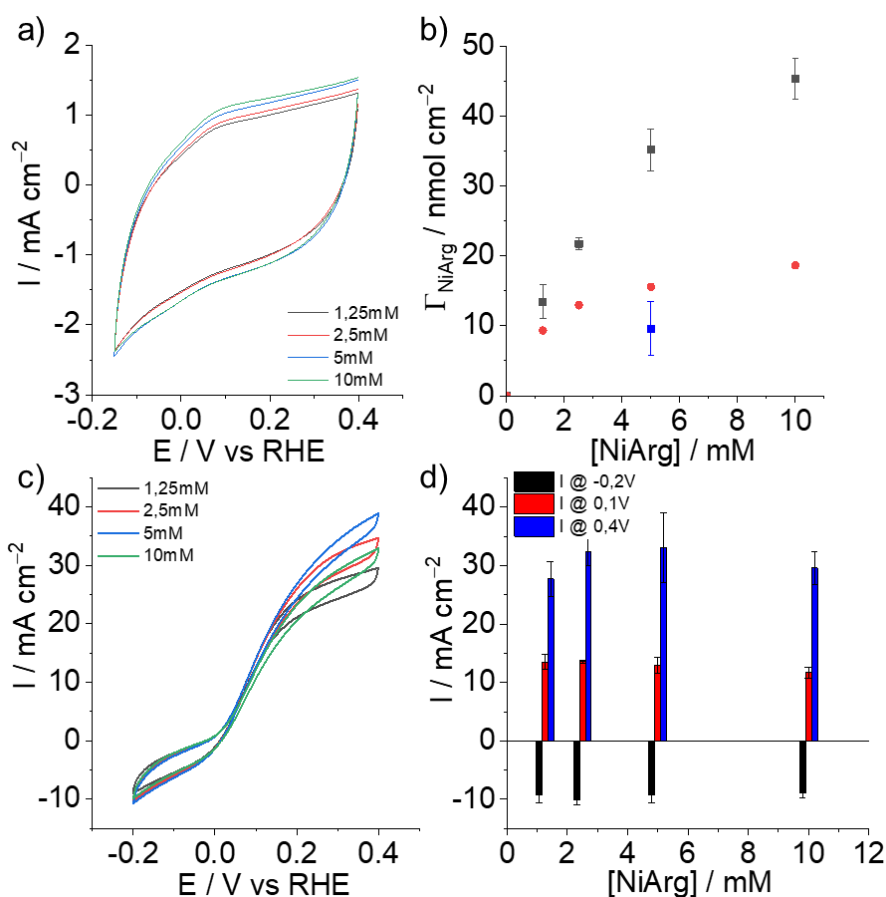

Figure 4: Electrochemical characterization of GDL|GA (0.4 mg cm^{-2}) electrodes at different **NiArg** loadings (2 µL of 1.25; 2.5; 5 and 10 mM) a) CV traces in 0.2 M phosphate buffer pH7 under argon (v = 20 mV s^{-1}) b) **NiArg** surface loadings determined from CV experiments (red dots) and from ICP-OES measurements before (black squares) and after (blue square) CV

measurements c) CV traces and d) corresponding current densities for HER at -0.2 V vs RHE and for HOR at 0.1 and 0.4 V vs RHE obtained from CVs in 0.5 M H_2SO_4 under argon and with a constant flow of H_2 at the back of the GDL (5 mL min^{-1}) (v = 20 mV s^{-1}) (See Figure S4 for other GA loadings.)

The catalytic performances of the GDL|GA electrodes (0.4 mg cm^{-2}) with different **NiArg** loading (Figure 4c) increase only slightly with the concentration of the **NiArg** deposition solution up to 5 mM, reaching 33 ± 6 mA cm^{-2} at 0.4V vs RHE.

$\Gamma_{\textbf{NiArg}}$ on GDL|GA|**NiArg** with lower GA loadings were also obtained from CVs experiments in neutral pH (Figure S5). As expected, similar trends were extracted for thinner GA films of 0.05, 0.1 and 0.2 mg cm^{-2} but with lower maximum Γ_{NiArg} values of 4.8, 9.8 and 12.4 nmol cm^{-2}, respectively (Figure 5). The surface loading $\Gamma_{\textbf{NiArg}}$ increases with solution concentration in **NiArg** following a simple Langmuir binding isotherm:

$$\Gamma_{NiArg} = Aq_{GA} \frac{K_{NiArg}\ [\text{NiArg}]}{1 + K\ [\text{NiArg}]}$$

Where A is the density of binding sites available the GA electrode (nmol mg^{-1}), q_{GA} the amount of GA deposited (mg cm^{-2}), $K_{\textbf{NiArg}}$ the association constant between **NiArg** and the GA electrode surface (L mol^{-1}) and [**NiArg**] the concentration of **NiArg** in the deposition solution (mol L^{-1}). The data could be fitted with a single $K_{\textbf{NiArg}}$ affinity constant for all series, underlining the effective grafting of the molecular catalyst to the GA modified electrode (Figure 5a). The $K_{\textbf{NiArg}}$ value of 640 L mol^{-1} is a low affinity binding constant, in coherence with a non-specific electrostatic interactions between the guanidinium groups of **NiArg** and the carboxylate of the GA surface. It is also possible that π-cations interactions takes place between the guanidinium moieties and the π-conjugated parts of the GA surface as already suggested with CNTs.
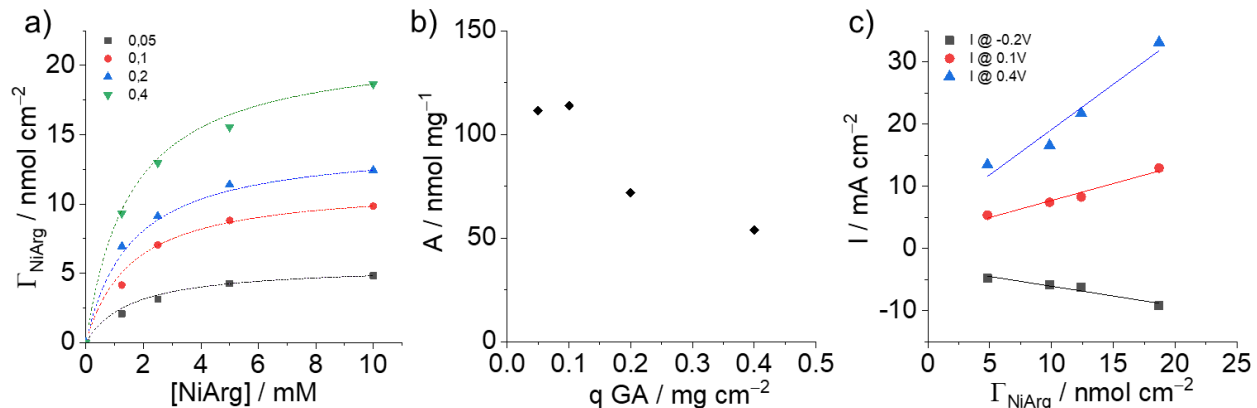
Figure 5: a) Γ_{NiArg} determined from CV experiments for GDL|GA electrodes with 0.05 (black squares), 0.1 (red dots), 0.2 (blue triangles) and 0.4 (green triangles) mg cm^{-2} of GA as function of the **[NiArg]** in the soaking solution, the dashed traces correspond to the fitted binding isotherm for each electrode thickness b) evolution of the site density as function of the amount of GA at the surface of the GDL c) Evolution of the values of HOR and HER catalytic currents (see Figure S4) from CV at -0.2 (black squares); 0.1 (red dots) and 0.4V vs RHE (blue triangles) with the Γ_{NiArg} extracted from CV at pH7 from GDL|GA electrodes with 0.05, 0.1, 0.2 and 0.4 mg cm^{-2} of GA incubated with 10 mM **NiArg**.

Interestingly, the A value, corresponding to the number of available anchoring sites per surface area, is decreasing with increasing GA loadings (Figure 5b). This indicates that anchoring site availability decreases with thicker GA deposits, which stems from a loss of porosity and clogging up of thicker GA deposit. Interestingly, the maximum catalytic current densities for both HER and HOR increase linearly with maximum Γ_{NiArg} taken at individual GA loadings (Figure 5c and S6). However, in the present series, further increase of GA loading leads to a decrease of the relative grafting site availability (Figure 5b) preventing a linear improvement of the catalyst loading and thus of the obtained catalytic currents (Figure 3a).

The stability of the best performing and mechanically stable GDL|GA|**NiArg** electrodes (0.4 mg cm^{-2} of GA and modified with a 5 mM solution of **NiArg**) was then studied in chronoamperometry (CA) for HOR at 0.1 and 0.3 V vs RHE (Figure 6a).
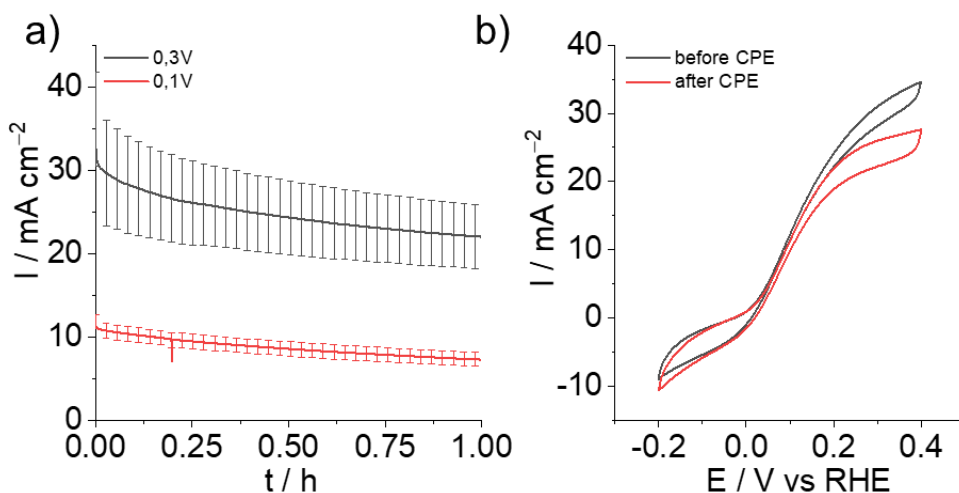

Figure 6: a) Averaged current values of the CA triplicates of the GDL|GA|**NiArg** modified electrodes at 0.3V (black trace) and 0.1V (red trace) and b) CV traces of the GDL|GA|**NiArg** before (black trace) and after (red trace) CA at 0.3V vs RHE in 0.5M H$_2$SO$_4$ under argon and with a constant flow of H$_2$ at the back of the GDL (5 mL min^{-1}) ($v = 20$ mV s^{-1})

At both applied potentials, a steady decrease could be observed for the GDL|GA|**NiArg** electrodes over the course of 1 h experiment, going from 31 ± 6 to 22 ± 5 mA cm^{-2} at 0.3 V vs RHE and from 11 ± 1 to 7 ± 1 mA cm^{-2} at 0.1 V vs RHE, retaining respectively 71 and 64% of catalytic activity (Figure 6a and S7). As mentioned above, loss of the catalyst through solution leaching can partly explain this decay and is consistent with the low calculated K$_{NiArg}$ value. XPS spectra recorded after electrocatalytic experiments also show that some of the catalyst could have potentially been oxidized at the phosphine ligand (Figure S9) which is another possible reason for nickel releasing out of the electrode. On the other hand, minimal changes are observed in the Ni 2p core level spectra, consisting of a small broadening of the main Ni 2p3/2 peak on the high

binding energy side. In addition, CVs performed before and after CA measurements showed slight modification in the electrocatalytic response, with a decrease of the HOR contribution combined with an increase of HER (Figure 6b). This hints that the decrease in HOR performance could also be due to electrode flooding overtime, hampering H_2 diffusion within the active layer rather than decomposition of **NiArg**. After 1h of electrolysis at 0.3V vs RHE, TOF_{HOR} between 3.3 and 11.9 s^{-1} can be estimated, taking the maximum and minimum values of $\Gamma_{\textbf{NiArg}}$ obtained through ICP measurements, respectively (see above).

Conclusion

We described the use of GA to prepare porous electrodes suitable for supported molecular electrocatalysis. The high degree of functionalization of GA allowed efficient incorporation of a bio-inspired nickel-based molecular catalyst through non-covalent electrostatic interactions. The high catalytic current densities, setting up new benchmark for molecular HOR, were achieved by optimization of the electrode design and catalyst loading. Further optimization of the catalytic layer is underway in order to (i) develop multivalent grafting to prevent leaching, (ii) maximize the number of available active sites through increased film thickness with retention of high porosity as well as (iii) rationalize formulation to prevent electrode flooding and increase the stability of the anode overtime. In the broader context of electrode nano-structuration, this work legitimates the use of GA as a versatile platform for supported molecular electrocatalysis with upscale potential similar to other graphene derivatives for preparation of large surface electrodes.

ASSOCIATED CONTENT

The following files are available free of charge.

Electronic supporting information (file type, i.e., PDF)

brief description (file type, i.e., PDF)

AUTHOR INFORMATION

Corresponding Authors

vincent.artero@cea.fr

Author Contributions

The manuscript was written through contributions of all authors. All authors have given approval to the final version of the manuscript.

Notes

Any additional relevant notes should be placed here.

ACKNOWLEDGMENT

REFERENCES

(1)   Armaroli, N.; Balzani, V. The Hydrogen Issue. *ChemSusChem* **2011**, *4*, 21–36.
(2)   Staffell, I.; Scamman, D.; Abad, A. V.; Balcombe, P.; Dodds, P. E.; Ekins, P.; Shah, N.; Ward, K. R. The Role of Hydrogen and Fuel Cells in the Global Energy System. *Energy Environ. Sci.* **2019**, *12*, 463–491.
(3)   Gordon, R. B.; Bertram, M.; Graedel, T. E. Metal Stocks and Sustainability. *PNAS* **2006**, *103*, 1209–1214.
(4)   Sealy, C. The Problem with Platinum. *Materials Today* **2008**, *11*, 65–68.
(5)   Brouzgou, A.; Song, S. Q.; Tsiakaras, P. Low and Non-Platinum Electrocatalysts for PEMFCs: Current Status, Challenges and Prospects. *Applied Catalysis B: Environmental* **2012**, *127*, 371–388.
(6)   Jaouen, F.; Jones, D.; Coutard, N.; Artero, V.; Strasser, P.; Kucernak, A. R. Platinum Group Metal | Toward Catalysts Free of PGM Elements for PEMFC. *Johnson Matthey Technol. Rev.* **2018**, *62*, 231–255.
(7)   Sheng, W.; Bivens, A. P.; Myint, M.; Zhuang, Z.; Forest, R. V.; Fang, Q.; Chen, J. G.; Yan, Y. Non-Precious Metal Electrocatalysts with High Activity for Hydrogen Oxidation Reaction in Alkaline Electrolytes. *Energy Environ. Sci.* **2014**, *7*, 1719–1724.
(8)   Zhuang, Z.; Giles, S. A.; Zheng, J.; Jenness, G. R.; Caratzoulas, S.; Vlachos, D. G.; Yan, Y. Nickel Supported on Nitrogen-Doped Carbon Nanotubes as Hydrogen Oxidation Reaction Catalyst in Alkaline Electrolyte. *Nat Commun* **2016**, *7*, 1–8.

(9)   Davydova, E. S.; Speck, F. D.; Paul, M. T. Y.; Dekel, D. R.; Cherevko, S. Stability Limits of Ni-Based Hydrogen Oxidation Electrocatalysts for Anion Exchange Membrane Fuel Cells. *ACS Catal.* **2019**, 6837–6845.

(10)   Palanker, V. S.; Gajyev, R. A.; Sokolsky, D. V. On Adsorption and Electro-Oxidation of Some Compounds on Tungsten Carbide; Their Effect on Hydrogen Electro-Oxidation. *Electrochimica Acta* **1977**, *22*, 133–136.

(11)   McIntyre, D. R.; Burstein, G. T.; Vossen, A. Effect of Carbon Monoxide on the Electrooxidation of Hydrogen by Tungsten Carbide. *Journal of Power Sources* **2002**, *107*, 67–73.

(12)   Nagai, M.; Yoshida, M.; Tominaga, H. Tungsten and Nickel Tungsten Carbides as Anode Electrocatalysts. *Electrochimica Acta* **2007**, *52*, 5430–5436.

(13)   Izhar, S.; Nagai, M. Cobalt Molybdenum Carbides as Anode Electrocatalyst for Proton Exchange Membrane Fuel Cell. *Journal of Power Sources* **2008**, *182*, 52–60.

(14)   Izhar, S.; Yoshida, M.; Nagai, M. Characterization and Performances of Cobalt–tungsten and Molybdenum–tungsten Carbides as Anode Catalyst for PEFC. *Electrochimica Acta* **2009**, *54*, 1255–1262.

(15)   Fontecilla-Camps, J. C.; Volbeda, A.; Cavazza, C.; Nicolet, Y. Structure/Function Relationships of [NiFe]- and [FeFe]-Hydrogenases. *Chem. Rev.* **2007**, *107*, 4273–4303.

(16)   Vincent, K. A.; Parkin, A.; Armstrong, F. A. Investigating and Exploiting the Electrocatalytic Properties of Hydrogenases. *Chem. Rev.* **2007**, *107*, 4366–4413.

(17)   Lubitz, W.; Ogata, H.; Rüdiger, O.; Reijerse, E. Hydrogenases. *Chem. Rev.* **2014**, *114*, 4081–4148.

(18)   Xu, L.; Armstrong, F. A. Optimizing the Power of Enzyme-Based Membrane-Less Hydrogen Fuel Cells for Hydrogen-Rich H2–air Mixtures. *Energy Environ. Sci.* **2013**, *6*, 2166–2171.

(19)   Lalaoui, N.; Poulpiquet, A. de; Haddad, R.; Goff, A. L.; Holzinger, M.; Gounel, S.; Mermoux, M.; Infossi, P.; Mano, N.; Lojou, E.; Cosnier, S. A Membraneless Air-Breathing Hydrogen Biofuel Cell Based on Direct Wiring of Thermostable Enzymes on Carbon Nanotube Electrodes. *Chem. Commun.* **2015**, *51*, 7447–7450.

(20)   So, K.; Kitazumi, Y.; Shirai, O.; Nishikawa, K.; Higuchi, Y.; Kano, K. Direct Electron Transfer-Type Dual Gas Diffusion H2/O2 Biofuel Cells. *J. Mater. Chem. A* **2016**, *4*, 8742–8749.

(21)   Plumeré, N.; Rüdiger, O.; Oughli, A. A.; Williams, R.; Vivekananthan, J.; Pöller, S.; Schuhmann, W.; Lubitz, W. A Redox Hydrogel Protects Hydrogenase from High-Potential Deactivation and Oxygen Damage. *Nature Chemistry* **2014**, *6*, 822–827.

(22)   Fourmond, V.; Stapf, S.; Li, H.; Buesen, D.; Birrell, J.; Rüdiger, O.; Lubitz, W.; Schuhmann, W.; Plumeré, N.; Léger, C. Mechanism of Protection of Catalysts Supported in Redox Hydrogel Films. *J. Am. Chem. Soc.* **2015**, *137*, 5494–5505.

(23)   Oughli, A. A.; Conzuelo, F.; Winkler, M.; Happe, T.; Lubitz, W.; Schuhmann, W.; Rüdiger, O.; Plumeré, N. A Redox Hydrogel Protects the O2-Sensitive [FeFe]-Hydrogenase from Chlamydomonas Reinhardtii from Oxidative Damage. *Angewandte Chemie International Edition* **2015**, *54*, 12329–12333.

(24)   Ciaccafava, A.; Infossi, P.; Ilbert, M.; Guiral, M.; Lecomte, S.; Giudici- Orticoni, M. T.; Lojou, E. Electrochemistry, AFM, and PM-IRRA Spectroscopy of Immobilized Hydrogenase: Role of a Hydrophobic Helix in Enzyme Orientation for Efficient H2 Oxidation. *Angewandte Chemie* **2012**, *124*, 977–980.

16

(25) Monsalve, K.; Mazurenko, I.; Gutierrez- Sanchez, C.; Ilbert, M.; Infossi, P.; Frielingsdorf, S.; Giudici- Orticoni, M. T.; Lenz, O.; Lojou, E. Impact of Carbon Nanotube Surface Chemistry on Hydrogen Oxidation by Membrane-Bound Oxygen-Tolerant Hydrogenases. *ChemElectroChem* **2016**, *3*, 2179–2188.

(26) Gentil, S.; Che Mansor, S. M.; Jamet, H.; Cosnier, S.; Cavazza, C.; Le Goff, A. Oriented Immobilization of [NiFeSe] Hydrogenases on Covalently and Noncovalently Functionalized Carbon Nanotubes for H2/Air Enzymatic Fuel Cells. *ACS Catal.* **2018**, *8*, 3957–3964.

(27) Alonso-Lomillo, M. A.; Rüdiger, O.; Maroto-Valiente, A.; Velez, M.; Rodríguez-Ramos, I.; Muñoz, F. J.; Fernández, V. M.; De Lacey, A. L. Hydrogenase-Coated Carbon Nanotubes for Efficient H2 Oxidation. *Nano Lett.* **2007**, *7*, 1603–1608.

(28) Mazurenko, I.; Monsalve, K.; Infossi, P.; Giudici-Orticoni, M.-T.; Topin, F.; Mano, N.; Lojou, E. Impact of Substrate Diffusion and Enzyme Distribution in 3D-Porous Electrodes: A Combined Electrochemical and Modelling Study of a Thermostable H 2 /O 2 Enzymatic Fuel Cell. *Energy & Environmental Science* **2017**, *10*, 1966–1982.

(29) Curtis, C. J.; Miedaner, A.; Ciancanelli, R.; Ellis, W. W.; Noll, B. C.; Rakowski DuBois, M.; DuBois, D. L. [Ni(Et2PCH2NMeCH2PEt2)2]2+ as a Functional Model for Hydrogenases. *Inorg. Chem.* **2003**, *42*, 216–227.

(30) Gloaguen, F.; Rauchfuss, T. B. Small Molecule Mimics of Hydrogenases: Hydrides and Redox. *Chem. Soc. Rev.* **2008**, *38*, 100–108.

(31) Liu, T.; DuBois, D. L.; Bullock, R. M. An Iron Complex with Pendent Amines as a Molecular Electrocatalyst for Oxidation of Hydrogen. *Nature Chemistry* **2013**, *5*, 228–233.

(32) Schilter, D.; Camara, J. M.; Huynh, M. T.; Hammes-Schiffer, S.; Rauchfuss, T. B. Hydrogenase Enzymes and Their Synthetic Models: The Role of Metal Hydrides. *Chem. Rev.* **2016**, *116*, 8693–8749.

(33) Brazzolotto, D.; Gennari, M.; Queyriaux, N.; Simmons, T. R.; Pécaut, J.; Demeshko, S.; Meyer, F.; Orio, M.; Artero, V.; Duboc, C. Nickel-Centred Proton Reduction Catalysis in a Model of [NiFe] Hydrogenase. *Nature Chemistry* **2016**, *8*, nchem.2575.

(34) Wilson, A. D.; Newell, R. H.; McNevin, M. J.; Muckerman, J. T.; Rakowski DuBois, M.; DuBois, D. L. Hydrogen Oxidation and Production Using Nickel-Based Molecular Catalysts with Positioned Proton Relays. *J. Am. Chem. Soc.* **2006**, *128*, 358–366.

(35) DuBois, M. R.; DuBois, D. L. The Roles of the First and Second Coordination Spheres in the Design of Molecular Catalysts for H2 Production and Oxidation. *Chem. Soc. Rev.* **2008**, *38*, 62–72.

(36) Smith, S. E.; Yang, J. Y.; DuBois, D. L.; Bullock, R. M. Reversible Electrocatalytic Production and Oxidation of Hydrogen at Low Overpotentials by a Functional Hydrogenase Mimic. *Angewandte Chemie International Edition* **2012**, *51*, 3152–3155.

(37) Wilson, A. D.; Shoemaker, R. K.; Miedaner, A.; Muckerman, J. T.; DuBois, D. L.; DuBois, M. R. Nature of Hydrogen Interactions with Ni(II) Complexes Containing Cyclic Phosphine Ligands with Pendant Nitrogen Bases. *PNAS* **2007**, *104*, 6951–6956.

(38) DuBois, D. L.; Bullock, R. M. Molecular Electrocatalysts for the Oxidation of Hydrogen and the Production of Hydrogen – The Role of Pendant Amines as Proton Relays. *European Journal of Inorganic Chemistry* **2011**, *2011*, 1017–1027.

(39)   O'Hagan, M.; Shaw, W. J.; Raugei, S.; Chen, S.; Yang, J. Y.; Kilgore, U. J.; DuBois, D. L.; Bullock, R. M. Moving Protons with Pendant Amines: Proton Mobility in a Nickel Catalyst for Oxidation of Hydrogen. *J. Am. Chem. Soc.* **2011**, *133*, 14301–14312.

(40)   O'Hagan, M.; Ho, M.-H.; Yang, J. Y.; Appel, A. M.; DuBois, M. R.; Raugei, S.; Shaw, W. J.; DuBois, D. L.; Bullock, R. M. Proton Delivery and Removal in [Ni(PR2NR′2)2]2+ Hydrogen Production and Oxidation Catalysts. *J. Am. Chem. Soc.* **2012**, *134,* 19409–19424.

(41)   Ginovska-Pangovska, B.; Dutta, A.; Reback, M. L.; Linehan, J. C.; Shaw, W. J. Beyond the Active Site: The Impact of the Outer Coordination Sphere on Electrocatalysts for Hydrogen Production and Oxidation. *Acc. Chem. Res.* **2014**, *47*, 2621–2630.

(42)   Jain, A.; Lense, S.; Linehan, J. C.; Raugei, S.; Cho, H.; DuBois, D. L.; Shaw, W. J. Incorporating Peptides in the Outer-Coordination Sphere of Bioinspired Electrocatalysts for Hydrogen Production. *Inorg. Chem.* **2011**, *50*, 4073–4085.

(43)   Jain, A.; Reback, M. L.; Lindstrom, M. L.; Thogerson, C. E.; Helm, M. L.; Appel, A. M.; Shaw, W. J. Investigating the Role of the Outer-Coordination Sphere in [Ni(PPh2NPh-R2)2]2+ Hydrogenase Mimics. *Inorg. Chem.* **2012**, *51*, 6592–6602.

(44)   Dutta, A.; Lense, S.; Hou, J.; Engelhard, M. H.; Roberts, J. A. S.; Shaw, W. J. Minimal Proton Channel Enables H2 Oxidation and Production with a Water-Soluble Nickel-Based Catalyst. *J. Am. Chem. Soc.* **2013**, *135*, 18490–18496.

(45)   Dutta, A.; DuBois, D. L.; Roberts, J. A. S.; Shaw, W. J. Amino Acid Modified Ni Catalyst Exhibits Reversible H2 Oxidation/Production over a Broad PH Range at Elevated Temperatures. *PNAS* **2014**, *111*, 16286–16291.

(46)   Dutta, A.; Roberts, J. A. S.; Shaw, W. J. Arginine-Containing Ligands Enhance H2 Oxidation Catalyst Performance. *Angew. Chem. Int. Ed.* **2014**, *53*, 6487–6491.

(47)   Dutta, A.; Ginovska, B.; Raugei, S.; Roberts, J. A. S.; Shaw, W. J. Optimizing Conditions for Utilization of an H2 Oxidation Catalyst with Outer Coordination Sphere Functionalities. *Dalton Trans.* **2016**, *45*, 9786–9793.

(48)   Li, F.; Yang, H.; Li, W.; Sun, L. Device Fabrication for Water Oxidation, Hydrogen Generation, and CO2 Reduction via Molecular Engineering. *Joule* **2018**, *2*, 36–60.

(49)   Coutard, N.; Kaeffer, N.; Artero, V. Molecular Engineered Nanomaterials for Catalytic Hydrogen Evolution and Oxidation. *Chem. Commun.* **2016**, *52*, 13728–13748.

(50)   Bullock, R. M.; Das, A. K.; Appel, A. M. Surface Immobilization of Molecular Electrocatalysts for Energy Conversion. *Chem. Eur. J.* **2017**, *23*, 7626–7641.

(51)   Dalle, K. E.; Warnan, J.; Leung, J. J.; Reuillard, B.; Karmel, I. S.; Reisner, E. Electro- and Solar-Driven Fuel Synthesis with First Row Transition Metal Complexes. *Chem. Rev.* **2019**, *119*, 2752–2875.

(52)   Blakemore, J. D.; Gupta, A.; Warren, J. J.; Brunschwig, B. S.; Gray, H. B. Noncovalent Immobilization of Electrocatalysts on Carbon Electrodes for Fuel Production. *J. Am. Chem. Soc.* **2013**, *135*, 18288–18291.

(53)   Downes, C. A.; Marinescu, S. C. Efficient Electrochemical and Photoelectrochemical H2 Production from Water by a Cobalt Dithiolene One-Dimensional Metal–Organic Surface. *J. Am. Chem. Soc.* **2015**, *137*, 13740–13743.

(54)   Hanna, C. M.; Sanborn, C. D.; Ardo, S.; Yang, J. Y. Interfacial Electron Transfer of Ferrocene Immobilized onto Indium Tin Oxide through Covalent and Noncovalent Interactions. *ACS Appl. Mater. Interfaces* **2018**, *10*, 13211–13217.

(55) Hanna, C. M.; Luu, A.; Yang, J. Y. Proton-Coupled Electron Transfer at Anthraquinone Modified Indium Tin Oxide Electrodes. *ACS Appl. Energy Mater.* **2019**, *2*, 59–65.

(56) Wadsworth, B. L.; Khusnutdinova, D.; Urbine, J. M.; Reyes, A. S.; Moore, G. F. Expanding the Redox Range of Surface-Immobilized Metallocomplexes Using Molecular Interfaces. *ACS Appl. Mater. Interfaces* **2019**.

(57) Maurin, A.; Robert, M. Noncovalent Immobilization of a Molecular Iron-Based Electrocatalyst on Carbon Electrodes for Selective, Efficient CO2-to-CO Conversion in Water. *J. Am. Chem. Soc.* **2016**, *138*, 2492–2495.

(58) Reuillard, B.; Warnan, J.; Leung, J. J.; Wakerley, D. W.; Reisner, E. A Poly(Cobaloxime)/Carbon Nanotube Electrode: Freestanding Buckypaper with Polymer-Enhanced H2-Evolution Performance. *Angew. Chem. Int. Ed.* **2016**, *55*, 3952–3957.

(59) Kaeffer, N.; Morozan, A.; Fize, J.; Martinez, E.; Guetaz, L.; Artero, V. The Dark Side of Molecular Catalysis: Diimine–Dioxime Cobalt Complexes Are Not the Actual Hydrogen Evolution Electrocatalyst in Acidic Aqueous Solutions. *ACS Catal.* **2016**, *6*, 3727–3737.

(60) Beiler, A. M.; Khusnutdinova, D.; Wadsworth, B. L.; Moore, G. F. Cobalt Porphyrin–Polypyridyl Surface Coatings for Photoelectrosynthetic Hydrogen Production. *Inorg. Chem.* **2017**, *56*, 12178–12185.

(61) Zhanaidarova, A.; Jones, S. C.; Despagnet-Ayoub, E.; Pimentel, B. R.; Kubiak, C. P. Re(TBu-Bpy)(CO)3Cl Supported on Multi-Walled Carbon Nanotubes Selectively Reduces CO2 in Water. *J. Am. Chem. Soc.* **2019**, *141*, 17270–17277.

(62) Kramer, W. W.; McCrory, C. C. L. Polymer Coordination Promotes Selective CO2 Reduction by Cobalt Phthalocyanine. *Chem. Sci.* **2016**, *7*, 2506–2515.

(63) Reuillard, B.; Ly, K. H.; Rosser, T. E.; Kuehnel, M. F.; Zebger, I.; Reisner, E. Tuning Product Selectivity for Aqueous CO2 Reduction with a Mn(Bipyridine)-Pyrene Catalyst Immobilized on a Carbon Nanotube Electrode. *J. Am. Chem. Soc.* **2017**, *139*, 14425–14435.

(64) Leung, J. J.; Vigil, J. A.; Warnan, J.; Edwardes Moore, E.; Reisner, E. Rational Design of Polymers for Selective CO2 Reduction Catalysis. *Angewandte Chemie* **2019**, *131*, 7779–7783.

(65) Goff, A. L.; Artero, V.; Jousselme, B.; Tran, P. D.; Guillet, N.; Métayé, R.; Fihri, A.; Palacin, S.; Fontecave, M. From Hydrogenases to Noble Metal–Free Catalytic Nanomaterials for H2 Production and Uptake. *Science* **2009**, *326*, 1384–1387.

(66) Tran, P. D.; Le Goff, A.; Heidkamp, J.; Jousselme, B.; Guillet, N.; Palacin, S.; Dau, H.; Fontecave, M.; Artero, V. Noncovalent Modification of Carbon Nanotubes with Pyrene-Functionalized Nickel Complexes: Carbon Monoxide Tolerant Catalysts for Hydrogen Evolution and Uptake. *Angewandte Chemie* **2011**, *123*, 1407–1410.

(67) Rodriguez- Maciá, P.; Dutta, A.; Lubitz, W.; Shaw, W. J.; Rüdiger, O. Direct Comparison of the Performance of a Bio-Inspired Synthetic Nickel Catalyst and a [NiFe]-Hydrogenase, Both Covalently Attached to Electrodes. *Angewandte Chemie International Edition* **2015**, *54*, 12303–12307.

(68) N. Huan, T.; T. Jane, R.; Benayad, A.; Guetaz, L.; D. Tran, P.; Artero, V. Bio-Inspired Noble Metal-Free Nanomaterials Approaching Platinum Performances for H 2 Evolution and Uptake. *Energy & Environmental Science* **2016**, *9*, 940–947.

(69) Gentil, S.; Lalaoui, N.; Dutta, A.; Nedellec, Y.; Cosnier, S.; Shaw, W. J.; Artero, V.; Le Goff, A. Carbon-Nanotube-Supported Bio-Inspired Nickel Catalyst and Its Integration in Hybrid Hydrogen/Air Fuel Cells. *Angew. Chem. Int. Ed.* **2017**, *56*, 1845–1849.

(70) Oughli, A. A.; Ruff, A.; Boralugodage, N. P.; Rodríguez-Maciá, P.; Plumeré, N.; Lubitz, W.; Shaw, W. J.; Schuhmann, W.; Rüdiger, O. Dual Properties of a Hydrogen Oxidation Ni-Catalyst Entrapped within a Polymer Promote Self-Defense against Oxygen. *Nature Communications* **2018**, *9*, 864.

(71) Tran, P. D.; Morozan, A.; Archambault, S.; Heidkamp, J.; Chenevier, P.; Dau, H.; Fontecave, M.; Martinent, A.; Jousselme, B.; Artero, V. A Noble Metal-Free Proton-Exchange Membrane Fuel Cell Based on Bio-Inspired Molecular Catalysts. *Chem. Sci.* **2015**, *6*, 2050–2053.

(72) Gentil, S.; Molloy, J. K.; Carrière, M.; Hobballah, A.; Dutta, A.; Cosnier, S.; Shaw, W. J.; Gellon, G.; Belle, C.; Artero, V.; Thomas, F.; Le Goff, A. A Nanotube-Supported Dicopper Complex Enhances Pt-Free Molecular H2/Air Fuel Cells. *Joule* **2019**, *3*, 2020–2029.

(73) Bakandritsos, A.; Pykal, M.; Błoński, P.; Jakubec, P.; Chronopoulos, D. D.; Poláková, K.; Georgakilas, V.; Čépe, K.; Tomanec, O.; Ranc, V.; Bourlinos, A. B.; Zbořil, R; Otyepka, M. Cyanographene and Graphene Acid: Emerging Derivatives Enabling High-Yield and Selective Functionalization of Graphene. ACS Nano 2017, 11, 2982–2991.

(74) Mosconi, D.; Blanco, M.; Gatti, T.; Calvillo, L.; Otyepka, M.; Bakandritsos, A.; Menna, E.; Agnoli, S.; Granozzi, G. Arene CH Insertion Catalyzed by Ferrocene Covalently Heterogenized on Graphene Acid. *Carbon* **2019**, *143*, 318–328.

(75) Blanco, M.; Mosconi, D.; Tubaro, C.; Biffis, A.; Badocco, D.; Pastore, P.; Otyepka, M.; Bakandritsos, A.; Liu, Z.; Ren, W.; Agnoli, S.; Granozzi, G. Palladium Nanoparticles Supported on Graphene Acid: A Stable and Eco-Friendly Bifunctional C–C Homo- and Cross-Coupling Catalyst. *Green Chem.* **2019**, *21* (19), 5238–5247.

(76) Blanco, M.; Mosconi, D.; Otyepka, M.; Medveď, M.; Bakandritsos, A.; Agnoli, S.; Granozzi, G. Combined High Degree of Carboxylation and Electronic Conduction in Graphene Acid Sets New Limits for Metal Free Catalysis in Alcohol Oxidation. *Chem. Sci.* **2019**, *10* (41), 9438–9445.

Table Of Content